Sacrificial nanofibrous composites provide instruction without impediment and enable functional tissue formation

Brendon M. Baker[a,b], Roshan P. Shah[a], Amy M. Silverstein[a,b], John L. Esterhai[a,c], Jason A. Burdick[b], and Robert L. Mauck[a,b,1]

[a]McKay Orthopaedic Research Laboratory, Department of Orthopaedic Surgery, Perelman School of Medicine, and [b]Department of Bioengineering, University of Pennsylvania, Philadelphia, PA 19104; and [c]Philadelphia VA Medical Center, Philadelphia, PA 19104

Edited by Shu Chien, University of California at San Diego, La Jolla, CA, and approved July 17, 2012 (received for review April 28, 2012)

The fibrous tissues prevalent throughout the body possess an ordered structure that underlies their refined and robust mechanical properties. Engineered replacements will require recapitulation of this exquisite architecture in three dimensions. Aligned nanofibrous scaffolds can dictate cell and matrix organization; however, their widespread application has been hindered by poor cell infiltration due to the tight packing of fibers during fabrication. Here, we develop and validate an enabling technology in which tunable composite nanofibrous scaffolds are produced to provide instruction without impediment. Composites were formed containing two distinct fiber fractions: slow-degrading poly(ε-caprolactone) and water-soluble, sacrificial poly(ethylene oxide), which can be selectively removed to increase pore size. Increasing the initial fraction of sacrificial poly(ethylene oxide) fibers enhanced cell infiltration and improved matrix distribution. Despite the removal of >50% of the initial fibers, the remaining scaffold provided sufficient instruction to align cells and direct the formation of a highly organized ECM across multiple length scales, which in turn led to pronounced increases in the tensile properties of the engineered constructs (nearly matching native tissue). This approach transforms what is an interesting surface phenomenon (cells on top of nanofibrous mats) into a method by which functional, 3D tissues (>1 mm thick) can be formed, both in vitro and in vivo. As such, this work represents a marked advance in the engineering of load-bearing fibrous tissues, and will find widespread applications in regenerative medicine.

anisotropy | electrospinning | nanofiber | tissue engineering | meniscus fibrocartilage

The structural organization of any tissue, along with its biochemical and cellular composition, is essential for specialized function. Biomaterial scaffolds for tissue repair can possess a variety of functionalities (1), but ultimately must serve as a template for the directed formation of functional tissue (2). Electrospinning from polymer solutions to generate micrometer- to nanometer-scale fibers has emerged as a prominent method for fabricating 3D scaffolds with tissue-like microstructures (3–5). In this process, a high voltage applied to a viscous polymer solution results in the formation of fibers via electrostatic charge repulsion; these fibers collected *en masse* result in a 3D fibrous network. An extensive library of polymers can be electrospun, spanning a range of stiffness and fiber diameters (50 nm to several microns), capturing the biologic diversity of fiber diameters within the cellular microenvironment (6, 7). Importantly, the alignment of electrospun fibers can also be controlled, generating scaffolds that mimic the organization of tissues where direction dependence (structural and mechanical anisotropy) is essential for function, including cardiac (8), neural (9), and orthopaedic tissues (6).

Despite the potential of these nanofibrous scaffolds in engineering 3D tissue structures, a significant limitation of most work to date is that the instructional capacity of these materials is limited to surface interactions, largely due the small pore size of such scaffolds resulting from the tight packing of small-diameter of fibers (10) - a problem that is exacerbated when fibers are organized into aligned arrays (11, 12). This small pore size hampers scaffold colonization by exogenously seeded cells or neighboring host cells upon implantation, relegating tissue formation to a surface phenomenon on all but very thin scaffolds (13, 14). Thus, though the fibrous topography of electrospun scaffolds can serve as an appropriate basis for engineering a wide array of anisotropic tissues, the challenge of generating fully cellularized 3D tissues has considerably hampered their widespread application thus far.

Results

To address this significant limitation, we developed electrospun composites containing a selectively removable "sacrificial" fiber fraction uniformly integrated into the 3D structure of the scaffold during fabrication (Fig. 1*A*). We hypothesized that the increase in pore size and void space resulting from the removal of this sacrificial element would hasten cell ingress, enable an increased and uniform cell density, and ultimately lead to the formation of highly organized 3D tissues with greater functional capacity. We devised an electrospinning system and methodology for fabricating composites containing uniformly integrated, but distinct, fiber populations of poly(ε-caprolactone) (PCL) and poly(ethylene oxide) (PEO). These materials were selected based on their stability profiles in the hydrated state: PCL degrades slowly via hydrolysis and functions as a persisting structural element, whereas noncross-linked PEO dissolves instantly upon hydration and serves as a sacrificial element (Fig. 1 *B* and *C*). A custom tri-jet electrospinning device was used to fabricate composites containing controlled and varied ratios of PEO and PCL fibers (Fig. S1). By adjusting only the number of PEO and PCL electrospinning sources, the resultant sacrificial fiber content could be tuned to 20%, 40%, or 60% of the initial scaffold mass without altering morphologic features of either fiber population (Fig. S1*D* and Fig. 1*D*). To examine changes in topography resulting from the inclusion and subsequent removal of sacrificial fibers, SEM was performed on composites following hydration and lyophilization. Increases in pore size after fiber removal were evident in scaffolds initially containing 60% PEO fibers by mass (Fig. 1 *E* and *F*).

Though this approach is applicable to numerous tissues whose cellular and extracellular organization is intrinsic to function, we chose here to focus on the knee meniscus (15). This tissue is

Author contributions: B.M.B., J.L.E., J.A.B., and R.L.M. designed research; B.M.B., R.P.S., and A.M.S. performed research; B.M.B., R.P.S., and A.M.S. analyzed data; and B.M.B. and R.L.M. wrote the paper.

The authors declare no conflict of interest.

This article is a PNAS Direct Submission.

[1]To whom correspondence should be addressed. E-mail: lemauck@mail.med.upenn.edu.

This article contains supporting information online at www.pnas.org/lookup/suppl/doi:10.1073/pnas.1206962109/-/DCSupplemental.

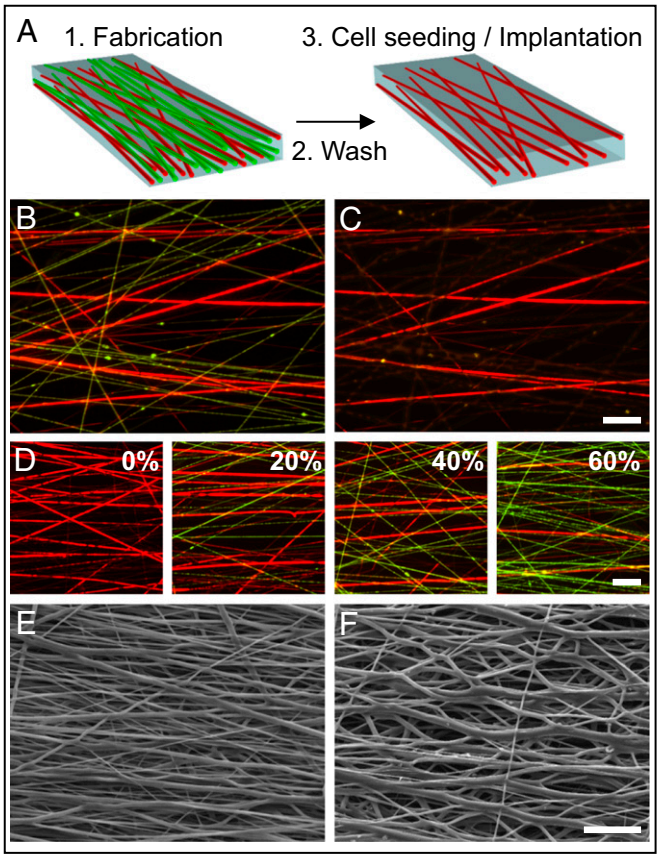

Fig. 1. Aligned composite nanofibrous scaffolds can be produced with a range of sacrificial fiber fractions. (*A*) Schematic depicting scaffold fabrication and subsequent removal of a sacrificial fiber subpopulation. (*B*) Slow-eroding PCL (fluorescently labeled red with Cell Tracker Red) and water-soluble PEO (fluorescently labeled green with fluorescein) fibers were coelectrospun into composite scaffolds. (*C*) Upon exposure to a humid environment, PEO fibers began to dissolve; further hydration completely removed these fibers from the composite. (*D*) Modulating the number of PCL and PEO sources produced composites with a range of sacrificial fiber inclusion (% indicates PEO content). SEM images of scaffolds containing low (0%) (*E*) and high (60%) (*F*) sacrificial fiber fractions after hydration. (Scale bars: 10 μm.)

composed of polarized cells embedded within a dense and highly aligned collagenous ECM. This architecture is necessary for the meniscus to carry out its physiologic role in load transmission; the ordered composition engenders robust and direction-dependent mechanical properties necessary to withstand the hoop stresses imposed upon the meniscus with normal locomotion. Indeed, the extreme mechanical conditions in which the meniscus operates predisposes it to traumatic injury (it is one of the most frequently injured musculoskeletal tissues), and a regenerative strategy for repairing or replacing the torn meniscus remains a major unmet clinical need. Toward that end, we used primary human meniscus cells, coupled with tunable nanofibrous composites, to produce mechanically functional meniscus replacement tissues.

In initial studies, composites with a range of sacrificial fiber content were seeded with cells derived from human meniscal tissue and cultured under free swelling conditions. Removal of the sacrificial fiber fraction decreased scaffold mechanical properties in a predictable fashion (Fig. S2*A*). As a result, constructs initially containing >40% PEO fiber fraction underwent cell-mediated deformations (unseeded controls did not contract; Fig. S2*B*). To maintain the planar form of the constructs, scaffold boundaries were constrained using custom fixtures throughout long-term culture (Fig. S2 *C–E*). Additional studies were performed to ensure that constructs arrayed in this fashion received equal nutrient supply, independent of positioning within the clamps. Under static culture conditions, considerably less cell division occurred in centrally located constructs (Fig. S2*F*, *Left*). Homogeneity in growth could be recovered, however, when constructs were maintained in dynamic conditions (gentle orbital shaking; Fig. S2*F*, *Right*). These dynamic conditions were used for all subsequent long-term studies.

Having established a suitable method for cultivating cell-seeded scaffolds with high sacrificial content (and therefore, low structural integrity), we next assessed whether the increases in pore size imparted by inclusion of sacrificial fibers could improve cellular colonization during long-term culture. To assess cell infiltration into the depths of the scaffolds, construct cross-sections were stained for cell nuclei (Fig. 2 *A* and *B*). In scaffolds lacking a sacrificial fiber fraction (0% PEO controls), cells were sequestered to the periphery, even after 12 wk of culture. With increasing sacrificial content, however, cell infiltration improved in a graded fashion, with 60% PEO constructs fully colonized (through the full depth of the >1-mm-thick scaffold) at 12 wk. To demonstrate the consistency of these findings across samples, the percentage of the total cell population located in the central 50% thickness was quantified by a semiautomated image analysis algorithm (16). The percentage of cells located in the center of scaffolds increased linearly with PEO content (R^2 of 0.999, $P < 0.001$; Fig. 2*D*), demonstrating that removal of the sacrificial fiber fraction improved cellular distribution within these 3D constructs. Additionally, the total number of cells in each construct was quantified and normalized to cross-sectional area (Fig. 2*F*). Constructs formed with high sacrificial content (60% PEO) possessed a twofold-higher cell density than pure PCL controls. Taken together, these results show that inclusion of high sacrificial content (60% PEO fibers by mass) encourages cell migration and division in these engineered 3D fibrous constructs, requisites for tissue formation during development as well as during tissue repair in the adult.

To ensure that the above findings were not specific to our in vitro culture conditions using meniscus-derived cells, we next assessed the in vivo colonization of acellular scaffolds following implantation. Scaffolds fabricated with a range of sacrificial PEO fiber fractions were implanted in dorsal s.c. pockets of Sprague–Dawley rats. After 4 wk, animals were euthanized and scaffolds along with adjacent tissue were resected, cryosectioned, and stained for cell nuclei. Upon gross dissection, composite scaffolds initially containing >40% sacrificial fiber content were well integrated with the surrounding host tissue. In controls lacking a sacrificial component (0% PEO), infiltrating cells were sequestered to the scaffold periphery and the bulk of the construct remained acellular (Fig. 3*A*). With increasing sacrificial content, the front of infiltrating cells approached the scaffold center, where the central regions of both 40% and 60% scaffolds were densely populated by host cells within 4 wk. Quantification of the percentage of cross-sectional area infiltrated by host cells demonstrated the consistency of these observations (Fig. 3*B*). It should be noted that the length of time required for full scaffold colonization was considerably shorter in this in vivo environment compared with our in vitro assessments, suggesting even greater efficacy of these scaffolds. Further, the threshold of sacrificial content required to enable full thickness colonization at this earlier time point was lower in vivo, because no difference in cell infiltration was observed between 40% and 60% PEO constructs. Although it may be necessary to tune the sacrificial content and timing depending on the application, these results evidence the need for a sacrificial component to enable rapid cellular colonization of nanofibrous scaffolds in vivo or in vitro.

For cell-mediated repair, both the total number of delivered cells and the functional capacity of each individual cell are determinants of success (17). The primary function of meniscus cells is to synthesize and maintain load-bearing ECM, which composes the bulk

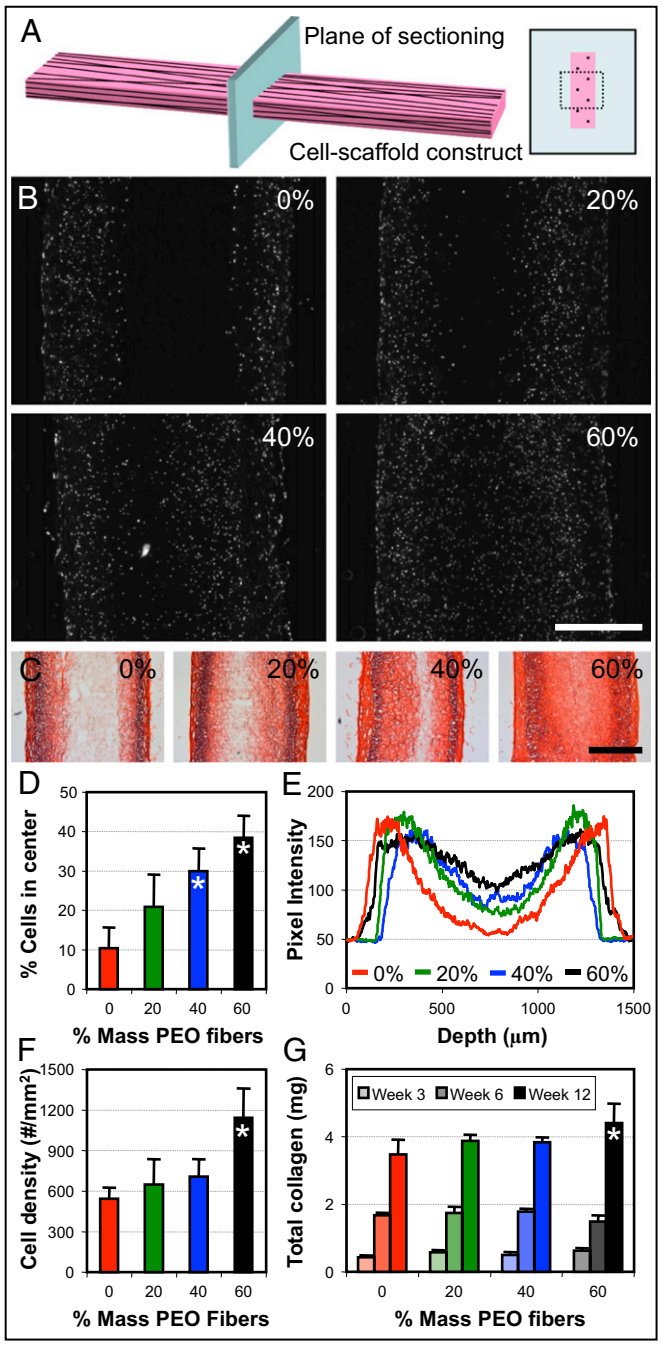

Fig. 2. Removal of sacrificial fibers promotes cell infiltration and improves matrix distribution in nanofibrous composites. Cross-sections (*A*) from constructs initially containing 0%, 20%, 40%, and 60% PEO (by mass) were stained with DAPI and Picrosirius Red to visualize cell nuclei (*B*) and collagen deposition (*C*), respectively. Representative sections are shown (Scale bar: 500 μm.) By week 12, higher initial fractions of sacrificial PEO fibers resulted in a greater percentage of cells within the central 50% of the construct (*D*), and a more homogeneous distribution of collagen through the scaffold depth (*E*). (*F*) Average cell density determined from week 12 DAPI-stained cross-sections increased with increasing sacrificial fiber content. (*G*) Collagen content increased with time in all groups, with 60% PEO constructs achieving higher levels compared with 0% controls by 12 wk of culture. All quantifications: $n = 5$ samples, $^*P < 0.05$ compared with time point-matched 0% constructs.

of meniscal tissue. To assess the functional capacity of infiltrated cells within these engineered constructs, we next examined the production and distribution of collagen, the predominant ECM component of load-bearing fibrous tissues. Paralleling the more even distribution of cells, the deposition of collagen became more homogeneous through the scaffold depth with increasing sacrificial content (Fig. 2*C*). In 0% PEO scaffolds, staining was completely absent in the central region of the scaffold. In contrast, collagen deposition was observed through the entire thickness of 60% PEO scaffolds. Densitometric profiles averaged across multiple samples demonstrated the consistency of these observations (Fig. 2*E*). No difference in collagen content was detected by biochemical assays across all groups at 3 and 6 wk of culture (Fig. 2*G*). However, by 12 wk, the total collagen content in 60% PEO constructs surpassed that of 0% controls ($P < 0.001$). Thus, the incorporation of sacrificial PEO fibers throughout the 3D scaffold led to not only a more homogeneous distribution of cells and matrix, but also increases in the overall content of this key tissue component.

The function of fibrocartilage arises not only from the abundance of the collagen-rich ECM, but additionally from the microstructural organization of this ECM (18). Indeed, scar tissue is rich in collagen, but the lack of order predisposes the repair site to failure (19, 20). Organization of electrospun fibers into linear arrays can preinstill mechanical and structural anisotropy into scaffolds (12, 21, 22), and countless studies have documented that cells encountering such aligned topographies will adopt a polarity reflecting the fiber organization. This instructional topography can likewise direct the organized deposition and resultant mechanics of ECM formed by surface-seeded cells (23). However, the organization of cells throughout the depth of infiltrated 3D constructs (rather than at the scaffold surface) has not previously been determined. Moreover, removal of a significant fraction of fibers, while enabling rapid cell infiltration, may diminish the capacity of the remaining fibers to instruct ECM organization. Substantiating this concern, qualitative assessment of SEM images indicated fiber dispersion increased in 60% PEO composites posthydration (Fig. 1*F*).

To examine the effect of sacrificial fiber content on the organization of cells that had infiltrated into the central regions of constructs, construct sections were taken *en face* (i.e., in the plane of the fibers), cell nuclei were stained, and the aspect ratio (long axis divided by short axis) and orientation of each nucleus was quantified (Fig. 4 *A–C*). Independent of sacrificial content, cell nuclei were elongated in the direction of fiber alignment and possessed a nuclear aspect ratio (NAR) of ~3; no difference was seen between 0% and 60% PEO constructs (Fig. 4*D*). Although nuclear morphology did not vary through the depth of constructs (Fig. S3*C*), the number of nuclei per field of view diminished with depth in 0% PEO controls in contrast to 60% PEO constructs (Fig. S3*B*). A similar analysis of human meniscus tissue yielded NAR values within the same range (~3; Fig. S4). In contrast, these same cells extracted from tissue and plated on tissue culture plastic or on the surface of aligned scaffolds possess NAR in the range of 1.5 to 2 (24, 25), suggesting that, like in native tissue, the 3D nanofibrous environment in both 0% and 60% PEO constructs promotes cell elongation in the fiber direction. Nuclear morphology, though indicative of cell elongation, does not necessarily prove that the instructive pattern persists with removal of sacrificial fibers. Thus, we next measured the angle between the long axis of each nucleus and the direction of fiber alignment (Fig. 4*E*, blue histograms). In 0% and 60% PEO scaffolds, nuclei were oriented in the direction of the surrounding fibers, with >75% of all cell nuclei aligned within ±15° of the fiber direction. It is not yet understood whether a high degree of nuclear organization provides a functional advantage in the context of matrix remodeling, or if this morphology simply results from physical constraints on the cell conferred by the surrounding matrix. Future studies mapping chromosomal territories in these cells may shed some light on the importance of nuclear shape and the organization of genes and regulatory regions within (26).

To determine whether this ordered cell polarity culminated in organized matrix production, the orientation of deposited collagen

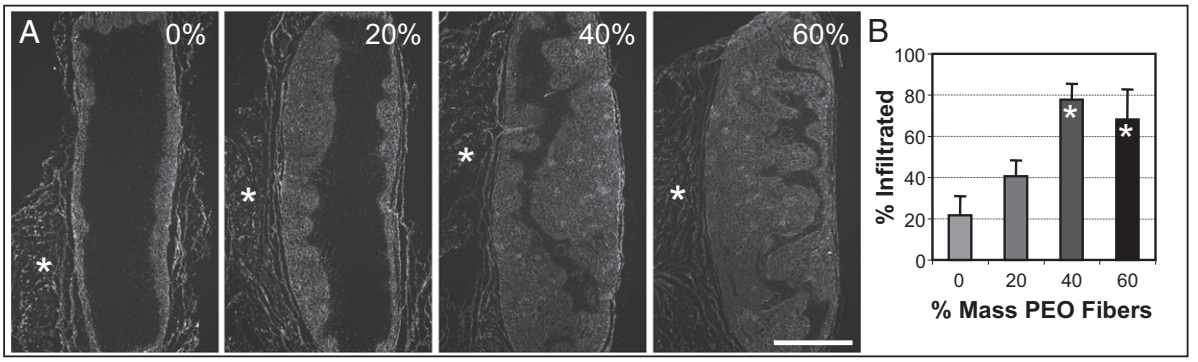

Fig. 3. Increasing sacrificial content improves scaffold colonization by host cells following s.c. implantation. (*A*) DAPI-stained cross-sections of 0%, 20%, 40%, and 60% PEO constructs harvested 4 wk after s.c. implantation (asterisks denote adjacent host tissue). (Scale bar: 1 mm.) (*B*) Quantification of the percentage of area of each scaffold cross-section infiltrated by host cells (n = 3 samples, $^*P < 0.05$ compared with 0% PEO constructs).

was next examined in *en face* sections using quantitative polarized light microscopy (Fig. 4*E*, *Insets*). This analysis showed that collagen organization in 0% and 60% PEO constructs was identical (Fig. 4*E*, orange histograms), and was more tightly coordinated with the alignment of surrounding nanofibers than was nuclear orientation. Paralleling the depth-dependent distribution of cell nuclei, the total amount of birefringence detected at a depth of 200 μm was notably higher in 60% PEO constructs than 0% controls (Fig. 4*E*, *Insets*). Transmission electron microscopy (TEM) of *en face* sections qualitatively confirmed these findings, revealing highly elongated cell bodies extended in the direction of nanofiber alignment, with dense arrays of collagen fibrils in this same prevailing direction (Fig. 5 *E* and *F* and Fig. S5). In transverse TEM images, collagen fibrils transected the plane of view and appeared as punctate bundles; fibrils running perpendicular to the direction of nanofiber alignment were not observed (Fig. 5 *A* and *B*). Ordered collagen fibrils and bundles occupied the majority of the extracellular space, occasionally interrupted by remnant PCL fibers (visualized as circular voids; Fig. 5 *B* and *D*, asterisks). The mechanism by which collagen fibrils form in an organized fashion remains poorly understood, although several reports indicate that initial cellular orientation plays an important role (27–29). Here, the nanofibrous template, even with very high sacrificial content, was sufficient to instruct cell morphology and subsequent matrix organization.

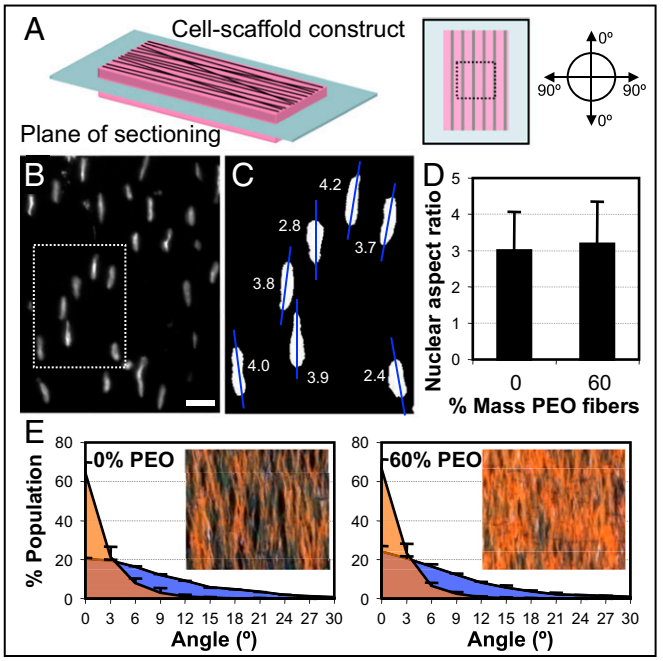

Fig. 4. Composite scaffolds with high sacrificial content retain their instructional capacity. (*A*) Sections were collected *en face* (in the plane of the fibers), ~200 μm from the surface of the construct. (*B*) DAPI-stained nuclei of 60% PEO constructs were elongated and aligned in the direction of the surrounding nanofibers. (Scale bar: 25 μm.) Fluorescent images were thresholded (*C*), and nuclear aspect ratio was determined in 12-wk 0% and 60% PEO constructs (*D*) (n = 3 samples per group, >1,000 nuclei analyzed per sample). (*E*) Distribution of nuclear (blue) and collagen (orange) orientation with respect to the fiber direction in 0% (*Left*) and 60% (*Right*) PEO constructs (n = 5 samples). (*Insets*) Representative Picrosirius Red-stained sections imaged under polarized light; coaligned birefringent ECM appears orange.

Though formation of anisotropic 3D tissue is a marked achievement, the ultimate goal of this work was to enhance the mechanical functionality of these engineered tissues. Fibrocartilaginous tissues such as the meniscus and annulus fibrosus function to convert compressive loads into tensile hoop stresses, which are borne by their dense network of aligned collagen fibers (18). As such, the tensile properties are an important parameter to assess in an engineered construct. Uniaxial tensile tests were performed to determine the modulus of constructs as a function of time in culture and initial sacrificial fiber content (Fig. 6*A*). At 3 wk, an inverse correlation between sacrificial fiber content and tensile modulus was observed. At this early time point, little collagen had been deposited, and so the measured properties reflected the baseline properties of the acellular scaffolds (Fig. S2*A*), where those with higher sacrificial content remained weaker. Following an additional 9 wk of culture, during which time a robust and uniform matrix was deposited, this trend reversed. At 12 wk, 60% PEO constructs possessed a significantly higher tensile modulus than 0% PEO controls. Stress-strain profiles of week 12 constructs demonstrate this improved mechanical functionality in 60% PEO constructs, across a physiologic strain range (Fig. 6*B*). To isolate the load-bearing contribution of newly synthesized ECM, the change in stiffness over the latter 9 wk of culture was quantified (Fig. 6*C*). Changes in construct stiffness with maturation increased nearly twofold more in samples with high sacrificial fiber content compared with those lacking sacrificial content ($P <$ 0.001). These results indicate that improvements in tissue function arose from enhanced construct cellularity and the resultant increases in collagen content and distribution. Indeed, increases in stiffness correlated significantly with cell density at the final time point (R^2 = 0.962, $P < 0.05$; Fig. S6). At the termination of this study, composites with the highest fraction of PEO fibers achieved a modulus of 48 ± 9 MPa, a value representing 73% of native tissue properties (66 ± 18 MPa) (30), and by far the highest yet reported for a tissue engineered meniscus construct.

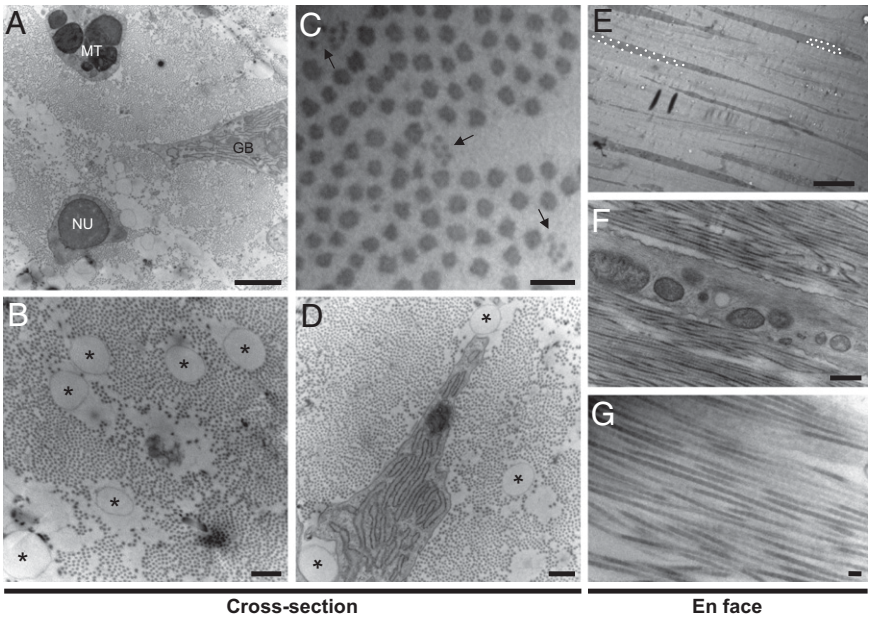

Fig. 5. Scaffolds direct the formation of a highly ordered microstructure consisting of polarized cells and aligned collagen fibrils. TEMs of week 12 construct sections taken transverse to (cross-section; *A–D*) or in the plane of the prevailing fiber direction (*en face*; *E–G*). Note that at these scales, where matrix was present, 0% and 60% PEO constructs were indistinguishable. (*A*) Construct cross-sections reveal cells embedded within a dense array of collagen fibrils (puncta). Nuclei (NU), mitochondria (MT), and Golgi bodies (GB) were frequently observed. (Scale bar: 2 μm.) (*B*) Residual PCL fibers (asterisks) appeared as circular voids, often adjacent to areas devoid of collagen fibrils. (Scale bar: 500 nm.) (*C*) Higher-magnification image of aligned collagen fibrils. Assembling (or disassembling) aggregates of collagen subfibrils (arrows) were occasionally observed. (Scale bar: 100 nm.) (*D*) Cells remained in intimate contact with nearby PCL fibers (asterisks) and newly formed collagen fibrils. (Scale bar: 500 nm.) (*E*) Low-magnification *en face* image confirms highly polarized cell bodies and elongated nuclei (outlined). (Scale bar: 10 μm.) (*F*) A cell extension ensconced tightly within aligned collagen fibers. (Scale bar: 500 nm.) (*G*) High-magnification view of aligned fibrils demonstrates ~67-nm periodic banding characteristic of collagen. (Scale bar: 100 nm.)

Discussion

This study outlines and validates a unique approach for the fabrication of engineered fibrous tissues that possess direction-dependent properties based on aligned electrospun composites with high sacrificial content. The selective removal of the sacrificial fiber fraction enabled cellular migration into the interior-most regions of scaffolds, and provided space for increased cellularity and ECM deposition. Despite the removal of more than half of the initial fiber content, the remaining material provided the necessary structural cues to direct alignment of infiltrated cells and the formation of a highly organized, mechanically functional ECM across multiple length scales. Though the mechanical properties of acellular scaffolds were inferior to native tissue, fully infiltrated constructs containing a higher cell density and greater ECM content achieved functional equivalence with native tissue. These findings illustrate the importance of striking a balance between the persistence of scaffolding material that can instruct organized tissue formation and the selective removal of impediments to tissue formation (i.e., the scaffold itself).

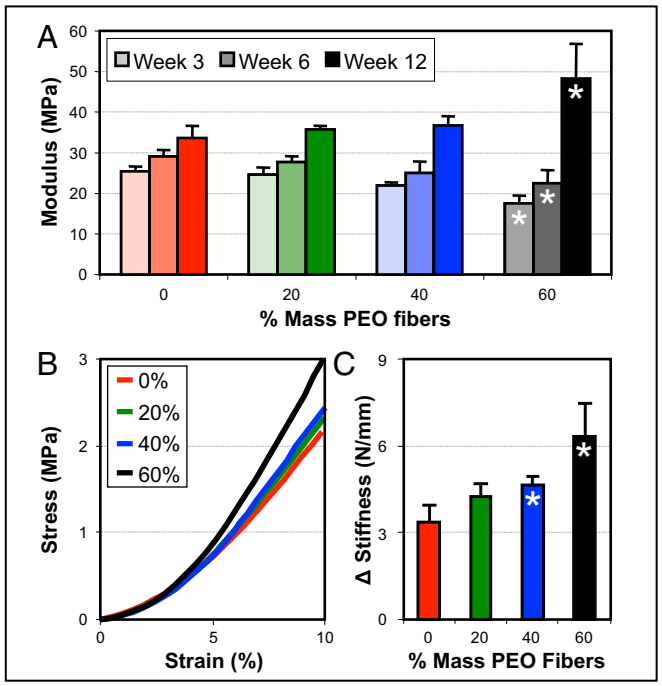

Fig. 6. Long-term culture of composite nanofibrous scaffolds with high sacrificial content results in improved mechanical function. (*A*) Tensile modulus of 0%, 20%, 40%, and 60% PEO constructs at 3, 6, and 12 wk of culture. (*B*) Average stress–strain response of week 12 constructs as a function of initial PEO content. (*C*) Change in stiffness over 12 wk of culture as a function of initial PEO content. All quantifications: $n = 5$ samples, $^*P < 0.05$ compared with time point-matched 0% constructs. Despite lower initial mechanical properties, constructs with high sacrificial fiber content engendered greater increases in tensile properties by the terminal time point.

Although the results presented here outline the functional ramifications of sacrificial content in composite nanofibrous scaffolds, and demonstrate the instructional capacity of these composites across multiple length scales, there remain additional modifications that could further improve their functionality. For instance, though ECM production and assembly occurs gradually, the sacrificial fibers used here disappeared instantly, well before cellular engraftment had occurred. Given the extensive palette of polymers that can be processed into fibrillar form by electrospinning, the use of a fiber population that erodes at a more moderate rate could simultaneously provide prolonged structural integrity (to thwart the effects of cell-mediated stresses at the boundaries) and yet degrade quickly enough to enable cell invasion and tissue formation in the newly vacated space (31). Alternatively, rather than simply relying on hydrolysis-mediated fiber degradation and removal, biologically responsive fibers (e.g., MMP cleavable) could be used to couple tissue ingrowth with scaffold degradation. Additionally, incorporation of exogenous growth factors or vectors within or on the fibers (32) or mechanical preconditioning may enhance the rate of tissue maturation, improving clinical relevance. Moreover, although 1-mm-thick tissues were formed in this study, larger 3D tissue structures may readily be formed using established multilamellar construction methods (33) and growth in dynamic, perfusion-based culture systems (10).

Whether scaffolds are seeded with cells in vitro, or implanted acellularly and infiltrated by host cells, rapid colonization will

be essential for tissue integration, maturation, and ultimately restoration of normal tissue function. As such, this work presents an enabling technology that transforms an interesting surface phenomenon (i.e., cells on top of nanofibrous mats) into a method by which organized 3D fiber-reinforced tissues, with native mechanical properties, can be formed in vitro or in vivo. Though the results here are presented in specific reference to the fibrocartilaginous knee meniscus, the approach may equally well be applied to any tissue in which ordered composition and direction-dependent properties underlie adult function, including skeletal and cardiac muscle, smooth muscle, and other fibrous tissues of the musculoskeletal system (i.e., tendons and ligaments, annulus fibrosus). As such, this work represents a marked advance in the engineering of load-bearing fibrous tissues, and will find widespread applications in regenerative medicine.

Materials and Methods

Please see *SI Text* for detailed descriptions of the histological and statistical analyses performed in these studies.

Nanofibrous Composite Fabrication. Aligned nanofibrous scaffolds containing two distinct but interspersed fiber populations were fabricated by coelectrospinning solutions of PCL (14.3% wt/vol in 1:1 tetrahydrofuran and *N,N*-dimethylformamide) and PEO (10% wt/vol in 90% ethanol). To tune fiber fractions, a custom apparatus was used to simultaneously electrospin from up to three sources onto a centrally located mandrel rotating at 10 m/s (Fig. S1) (31). By modulating the number of PCL and PEO sources, while maintaining a 2-mL/h flow rate, scaffolds composed of 0%, 20%, 40%, and 60% PEO fibers by mass were fabricated. In some studies, PCL and PEO solutions were doped with Cell Tracker Red (0.0005% wt/vol) or fluorescein (0.5% wt/vol), respectively, to permit fluorescent visualization. Scaffolds were also imaged with a Philips XL 20 SEM after lyophilization to visualize fiber and pore structure.

Cell Isolation and Construct Formation. Human meniscus fibrochondrocytes (MFCs) from two donors were isolated and expanded to passage 6 as in Baker et al. (14). Scaffolds (50 × 5 mm, with the long axis in the direction of fiber alignment) were hydrated in decreasing concentrations of ethanol (100%, 70%, 50%, 30% vol/vol), concluding with two washes in PBS, dissolving the PEO fibers. Each side received a 100-μL aliquot containing 5×10^5 MFCs followed by 1 h of incubation to allow for cell attachment. Constructs were cultured in chemically defined medium containing 10 ng/mL TGF-β3 changed twice weekly as in Baker and Mauck (23). One week after seeding, constructs were transferred to custom polysulfone fixtures and cultured on an orbital shaker (48 rpm; Fig. S2).

Mechanical and Biochemical Analyses. Before testing, sample cross-sectional area was determined with a laser-based measurement system. Tensile testing was performed with an Instron 5848 MicroTester. Samples (n = 5) were preloaded to 0.1 N for 60 s, then extended to failure at a rate of 0.1% of the gauge length per second; gauge length was maintained at 20 mm across all groups and time points. Stiffness was determined over a 1% strain range within the linear region of the force–elongation curve. Young's modulus was calculated from the corresponding stress–strain curve and the specimen geometry. Following tensile testing, collagen content was determined via the hydroxyproline assay (23).

Subcutaneous Implantation. Acellular scaffolds were implanted s.c. in male Sprague–Dawley rats (63–67 d, 276–300 g) at four sites just lateral to the dorsal midline at the shoulders and hips of each animal. Under anesthesia, rat dorsa were shaved, sterilized, and draped, and an incision was made. Each rat (n = 3) received a sterilized 1-mm-thick, 5 × 7 mm rectangular 0%, 20%, 40%, or 60% (wt/wt) PEO scaffold, with the placement randomized. Animals were monitored postoperatively for signs of pain and discomfort. Food and water were provided ad libitum. All animal procedures were approved by the Animal Component of Research Protocol Review Committee of the Philadelphia VA Medical Center.

ACKNOWLEDGMENTS. This work was supported by National Institutes of Health Grant R01 AR056624 and Department of Veterans Affairs Grant I01 RX000174. The views expressed in this article are those of the authors and do not necessarily reflect the position or policy of the Department of Veterans Affairs or the United States government. Additional support was provided by the Penn Center for Musculoskeletal Disorders and a National Science Foundation Graduate Research Fellowship (to B.M.B.).

1. Place ES, Evans ND, Stevens MM (2009) Complexity in biomaterials for tissue engineering. *Nat Mater* 8:457–470.
2. Macchiarini P, et al. (2008) Clinical transplantation of a tissue-engineered airway. *Lancet* 372:2023–2030.
3. Pham QP, Sharma U, Mikos AG (2006) Electrospinning of polymeric nanofibers for tissue engineering applications: A review. *Tissue Eng* 12:1197–1211.
4. Burger C, Hsiao BS, Chu B (2006) Nanofibrous materials and their applications. *Annu Rev Mater Res* 36:333–368.
5. Huang Z-M, Zhang Y-Z, Kotaki M, Ramakrishna S (2003) A review on polymer nanofibers by electrospinning and their applications in nanocomposites. *Compos Sci Technol* 63:2223–2253.
6. Mauck RL, et al. (2009) Engineering on the straight and narrow: The mechanics of nanofibrous assemblies for fiber-reinforced tissue regeneration. *Tissue Eng Part B Rev* 15:171–193.
7. Barnes CP, Sell SA, Boland ED, Simpson DG, Bowlin GL (2007) Nanofiber technology: Designing the next generation of tissue engineering scaffolds. *Adv Drug Deliv Rev* 59:1413–1433.
8. Shin M, Ishii O, Sueda T, Vacanti JP (2004) Contractile cardiac grafts using a novel nanofibrous mesh. *Biomaterials* 25:3717–3723.
9. Yang F, Murugan R, Wang S, Ramakrishna S (2005) Electrospinning of nano/micro scale poly(L-lactic acid) aligned fibers and their potential in neural tissue engineering. *Biomaterials* 26:2603–2610.
10. Pham QP, Sharma U, Mikos AG (2006) Electrospun poly(ε-caprolactone) microfiber and multilayer nanofiber/microfiber scaffolds: Characterization of scaffolds and measurement of cellular infiltration. *Biomacromolecules* 7:2796–2805.
11. Moffat KL, et al. (2009) Novel nanofiber-based scaffold for rotator cuff repair and augmentation. *Tissue Eng Part A* 15:115–126.
12. Li W-J, Mauck RL, Cooper JA, Yuan X, Tuan RS (2007) Engineering controllable anisotropy in electrospun biodegradable nanofibrous scaffolds for musculoskeletal tissue engineering. *J Biomech* 40:1686–1693.
13. Telemeco TA, et al. (2005) Regulation of cellular infiltration into tissue engineering scaffolds composed of submicron diameter fibrils produced by electrospinning. *Acta Biomater* 1:377–385.
14. Baker BM, Nathan AS, Huffman GR, Mauck RL (2009) Tissue engineering with meniscus cells derived from surgical debris. *Osteoarthritis Cartilage* 17:336–345.
15. Arnoczky SP (1999) Building a meniscus. Biologic considerations. *Clin Orthop Relat Res* 367(Suppl):S244–S253.
16. Baker BM, et al. (2008) The potential to improve cell infiltration in composite fiber-aligned electrospun scaffolds by the selective removal of sacrificial fibers. *Biomaterials* 29:2348–2358.
17. Gilbert PM, et al. (2010) Substrate elasticity regulates skeletal muscle stem cell self-renewal in culture. *Science* 329:1078–1081.
18. Setton LA, Guilak F, Hsu EW, Vail TP (1999) Biomechanical factors in tissue engineered meniscal repair. *Clin Orthop Relat Res* 367(Suppl):S254–S272.
19. Beredjiklian PK, et al. (2003) Regenerative versus reparative healing in tendon: A study of biomechanical and histological properties in fetal sheep. *Ann Biomed Eng* 31:1143–1152.
20. Newman AP, Anderson DR, Daniels AU, Dales MC (1989) Mechanics of the healed meniscus in a canine model. *Am J Sports Med* 17:164–175.
21. Ayres CE, et al. (2007) Incremental changes in anisotropy induce incremental changes in the material properties of electrospun scaffolds. *Acta Biomater* 3:651–661.
22. Courtney T, Sacks MS, Stankus J, Guan J, Wagner WR (2006) Design and analysis of tissue engineering scaffolds that mimic soft tissue mechanical anisotropy. *Biomaterials* 27:3631–3638.
23. Baker BM, Mauck RL (2007) The effect of nanofiber alignment on the maturation of engineered meniscus constructs. *Biomaterials* 28:1967–1977.
24. Nathan AS, Baker BM, Nerurkar NL, Mauck RL (2011) Mechano-topographic modulation of stem cell nuclear shape on nanofibrous scaffolds. *Acta Biomater* 7:57–66.
25. Heo SJ, et al. (2011) Fiber stretch and reorientation modulates mesenchymal stem cell morphology and fibrous gene expression on oriented nanofibrous microenvironments. *Ann Biomed Eng* 39:2780–2790.
26. Cremer T, Cremer C (2001) Chromosome territories, nuclear architecture and gene regulation in mammalian cells. *Nat Rev Genet* 2:292–301.
27. Wang JH, Jia F, Gilbert TW, Woo SL (2003) Cell orientation determines the alignment of cell-produced collagenous matrix. *J Biomech* 36:97–102.
28. Li S, Van Den Diepstraten C, D'Souza SJ, Chan BMC, Pickering JG (2003) Vascular smooth muscle cells orchestrate the assembly of type I collagen via α2β1 integrin, RhoA, and fibronectin polymerization. *Am J Pathol* 163:1045–1056.
29. Manwaring ME, Walsh JF, Tresco PA (2004) Contact guidance induced organization of extracellular matrix. *Biomaterials* 25:3631–3638.
30. Bursac P, York A, Kuznia P, Brown LM, Arnoczky SP (2009) Influence of donor age on the biomechanical and biochemical properties of human meniscal allografts. *Am J Sports Med* 37:884–889.
31. Baker BM, Nerurkar NL, Burdick JA, Elliott DM, Mauck RL (2009) Fabrication and modeling of dynamic multipolymer nanofibrous scaffolds. *J Biomech Eng* 131:101012.
32. Phillips JE, Burns KL, Le Doux JM, Guldberg RE, García AJ (2008) Engineering graded tissue interfaces. *Proc Natl Acad Sci USA* 105:12170–12175.
33. Nerurkar NL, et al. (2009) Nanofibrous biologic laminates replicate the form and function of the annulus fibrosus. *Nat Mater* 8:986–992.